Contributions to Mineralogy and Petrology (2023) 178:8
https://doi.org/10.1007/s00410-022-01989-4

ORIGINAL PAPER

On the interpretation of TitaniQ and ZiR thermobarometry in subduction complexes

Frank S. Spear[1] · Oliver M. Wolfe[1] · John T. Cheney[2]

Received: 7 October 2022 / Accepted: 20 December 2022

Abstract

Titanium and zirconium analyses of quartz and rutile from blueschist samples from the eclogite–blueschist unit (EBU) in northern Sifnos, Greece, have been evaluated to determine the extent to which the intersection of the Ti-in-quartz (TitaniQ) and zirconium-in-rutile (ZiR) thermometers reflect peak metamorphic P–T conditions. Ti concentrations range from 100 to 530 ppb and Zr concentrations range from 14 to 44 ppm; there is no significant zoning observed in any grains and no significant differences in concentrations in samples south and north of the Vroulidia shear zone (VSZ). Lines of equal Keq from the TitaniQ and ZiR thermometers intersect at around 450–500 °C and 2.2–2.4 GPa, which is similar to the peak metamorphic conditions of 530 °C, 1.9 GPa for samples north of the VSZ. However, the intersection is inconsistent with the peak metamorphic conditions of 525 °C, 1.1–1.4 GPa for samples south of the VSZ even when TitaniQ temperatures are corrected for reduced activity of TiO_2. Rather, TitaniQ temperatures are consistent with Ti values being incorporated into quartz during prograde metamorphism along a subduction geotherm of 10–12 deg/km at around 300 °C. ZiR temperatures are consistent with rutile nucleation and growth at around 450–500 °C along a similar metamorphic geotherm after the rutile-in reaction was overstepped by around 1 kJ/mol-O. The TitaniQ and ZiR thermometers do not, therefore, reflect peak metamorphic P–T conditions in these rocks but rather record recrystallization or growth processes during prograde subduction.

Keywords Ti-in-quartz thermometry · TitaniQ · Zr-in-rutile thermometry · ZiR · Quartz in garnet barometry · QuiG · Trace element thermometry · Blueschists

Introduction

Trace element thermobarometry has the potential in metamorphic studies of revealing details about the P–T history experienced by a rock. They are generally simple to use and, because they involve trace elements, are not overly sensitive to compositional non-ideality. Two trace element thermobarometers, Ti-in-quartz (TitaniQ) and Zr-in-rutile (ZiR), are particularly useful in the study of blueschists because of the near ubiquity of quartz and rutile and because at the P–T conditions of interest, intracrystalline diffusion is sufficiently slow that the trace element concentrations are not greatly altered during exhumation (e.g., Cherniak et al. 2007a, b). Additionally, TitaniQ and ZiR are both pressure dependent equilibria but to different degrees so that isopleths of Ti-in-quartz and Zr-in-rutile intersect at a unique point on a P–T diagram (e.g., Thomas et al. 2010; Osborne et al. 2022).

The question remains, however, as to how best to interpret the P–T conditions recorded by these thermobarometers. Osborne et al. (2022, Fig. 8a) show a P–T diagram with isopleths of Ti-in-quartz and Zr-in-rutile for four of their experiments. The isopleths intersect at P–T conditions very similar to the experimental conditions, supporting the inference that these two thermobarometers can faithfully record peak metamorphic conditions. Similarly, Thomas et al. (2010, Fig. 9) present a plot of Zr-in-rutile and Ti-in-quartz for a sample of blueschist from Sifnos, Greece. The two thermobarometers intersected in a region of P–T space at around 2.2 ± 0.25 GPa and 560 ± 15 °C, which is remarkably consistent with the peak metamorphic conditions inferred for

Communicated by Mark S Ghiorso.

✉ Frank S. Spear
spearf@rpi.edu

[1] Department of Earth and Environmental Sciences, Rensselaer Polytechnic Institute, 110 8th Street, Troy, NY 12180, USA

[2] Department of Geology, Amherst College, 220 South Pleasant Street, Amherst, MA 01002, USA

Published online: 05 January 2023

these rocks from by Castro and Spear (2017), which again supports the suggestion that these two thermobarometers reliably record the peak metamorphic conditions.

Whereas it is tempting to interpret the results from the Sifnos blueschists (Thomas et al. 2010) as indication that together TitaniQ and ZiR faithfully record the peak metamorphic conditions in these rocks, there are several lines of evidence to suggest that the intersection of these two thermobarometers at conditions near the inferred metamorphic peak is serendipitous. This paper presents an analysis of the petrologic evolution of several well-characterized samples from the EBU of Sifnos to demonstrate that these thermobarometers in fact record the conditions of quartz and rutile nucleation and growth (i.e., formation), which do not occur at the same P–T conditions and do not occur at the metamorphic peak. Although it is perhaps disappointing that these thermobarometers do not record peak conditions, careful analysis of the petrogenesis of samples in which these thermobarometers are found can help constrain the prograde P–T path, which is of considerable value in evaluating subduction geotherms and tectonic evolution.

Methods

Zr analyses in rutile were made on the Cameca SX-100 electron microprobe at Rensselaer Polytechnic Institute as was reported by Spear et al. (2006) and precisions ranged from 7 to 13 ppm, depending on the analytical protocol adopted. Ti analyses in quartz were obtained using the IMS 3f at Woods Hole Oceanographic Institute. Cores approximately 1 cm diameter were drilled out of polished thin sections and remounted in a single 1inch epoxy round so that all quartz grains to be analyzed could be in the IMS 3f chamber at the same time. Cores were drilled that included both matrix quartz and quartz inclusions in garnet. A working curve was generated using the QTiP suite of synthetic Ti-in-quartz standards (Thomas et al. 2010) and was forced through the origin. Analytical precisions were on the order of tens of ppb and the overall accuracy was estimated to be approximately ± 0.1 ppm (100 ppb).

Thermobarometric calculations for the solubility of Ti in quartz were done using the calibration of Osborne et al. (2022) and Thomas et al. (2010). Both calibrations give identical temperatures (to within 1 °C) at approximately 1.0 GPa but the Osborne et al. (2022) calibration yields lower temperatures at higher and lower pressures due to the pressure dependence of the $\Delta V_{reaction}$ term. Only the results using the Osborne et al. (2022) calibration are shown, but the choice of thermometer calibrations does not in any way impact the results of this study. Calculations for the solubility of Zr in rutile were done using the calibration of Tomkins et al. (2007). Mineral assemblage diagrams (MADs or pseudosections) were calculated on each sample to provide an estimate of the equilibrium phase boundary for rutile. Calculations were performed using the thermodynamic datasets of Holland and Powell (2011: HP11; ds6.2), Holland and Powell (1998: HP98; ds 5.5) and Spear and Pyle (2010: SPaC) in order to compare results. All calculations were done using program Gibbs (Spear and Wolfe 2022: supplemental material).

Sample setting

The geologic setting of the EBU of northern Sifnos has been described in detail by Spear et al. (2006), Roche et al. (2016), and Castro and Spear (2017) and the reader is referred to these papers and references therein for additional details. The samples discussed in the present study (Fig. 1 and Table 1) were analyzed for zirconium-in-rutile by Spear et al. (2006) and for quartz-in-garnet barometry by Castro and Spear (2017) (samples SPH99-1, SPH99-5 and SPH99-7). It is particularly important to note the location of the Vroulidia shear zone (VSZ) and that five samples are located to the south and four sample locations are to the north of the VSZ (Fig. 1 and Table 1). Castro and Spear (2017) reported significantly different P–T conditions for garnet nucleation and growth for samples south and north of the VSZ, as will be discussed in detail below.

Results

Analyses of Zr in rutile and Ti in quartz for the suite of samples are presented in Tables 2 and 3. Values of Zr in rutile range from 13 to 43 ppm in samples south of the VSZ and

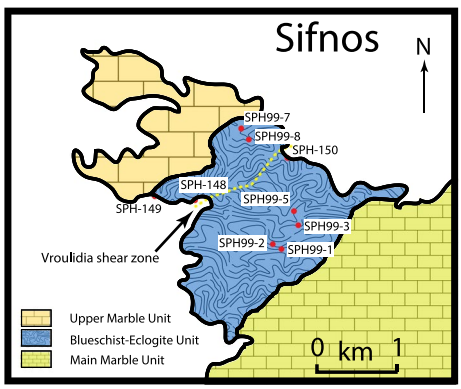

Fig. 1 Geologic map of the north end of Sifnos, Greece, showing the location of samples in the Blueschist–Eclogite Unit relative to the Vroulidia shear zone (VSZ). Map is modified from Spear et al. (2014), Castro and Spear (2017), and Roche et al. (2016). Coordinates for upper left and lower right of the map are, respectively, Lat = 37.04376°, Long = 24.62947°; Lat = 37.00224°, Long = 24.68514°

Table 1 Mineral assemblages in blueschist samples from Sifnos, Greece (modified from Spear et al. 2006)

Sample	Latitude	Longitude	Rock type	Minerals present	Comments
Samples south of the Vroulidia shear zone					
SPH99-1c	37.01689	24.66733	Metapelite	Grt + Phn + Pg + Qtz + Rt + Zrn + Gln + Ep + (Ab + Mt)	Ab + Mt "clots" are pseudomorphs
SPH99-2	37.01748	24.66581	Metapelite	Grt + Phn + Pg + Cld (in Grt) + Qtz + Rt + Zrn + Gln + Ep + (Ab + Mt)	Ab + Mt "clots" are pseudomorphs
SPH99-3	37.02013	24.67006	Metapelite	Grt + Phn + Pg + Cld (in Grt) + Qtz + Rt + Zrn + Ep + (Ab + Mt)	Ab + Mt "clots" are pseudomorphs
SPH99-5	37.02178	24.66924	Metapelite	Grt + Phn + Pg + Cld (in Grt) + Qtz + Rt + Zrn + Gln + Ep + (Ab + Mt)	Ab + Mt "clots" are pseudomorphs; Clinozoisite lineation inside garnet
SPH-150	37.02811	24.66784	Metapelite	Grt + Phn + Pg + Qtz + Rt + Zrn + Gln + (Ab + Mt) + Ank	Ab + Mt "clots" are pseudomorphs
Samples north of the Vroulidia shear zone					
SPH99-7	37.03224	24.66068	Metabasite	Grt + Jd + Gln + Ep + Rt + Sph + Pg + Phn + Qtz + Zrn	Rutile in garnet only; sphene in matrix
SPH99-8a	37.03078	24.66188	Metapelite	Grt + Phn + Pg + Qtz + Rt + Zrn + Gln + Ep + (Ab + Mt)	Ab + Mt "clots" are pseudomorphs
SPH99-8b	37.03078	24.66188	Metapelite	Grt + Phn + Pg + Omp (in Grt) + Qtz + Rt + Zrn + Gln + Ep + (Ab + Mt)	Ab + Mt "clots" are pseudomorphs
SPH-148a	37.02319	24.65279	Metabasite	Grt + Omp + Gln + Ep + Rt + Sph + Pg + Phn + Qtz + Zrn + Ank	Rutile in garnet only; sphene in matrix
SPH-148c	37.02319	24.65279	Metabasite	Grt + Omp + Gln + Ep + Rt + Sph + Pg + Phn + Zrn + Ank	Rutile in garnet only; sphene in matrix
SPH-149c	37.02364	24.64679	Metabasite	Grt + Omp + Gln + Ep + Rt + Sph + Pg + Phn + Qtz + Zrn	Rutile in garnet only; sphene in matrix
SPH-149d	37.02364	24.64679	Metapelite	Grt + Jd + Gln + Rt + Pg + Phn + Chl + Qtz + Zrn	Pseudomorph clusters of Rt + Zrn + silicates

Grt garnet; *Qtz* quartz; *Phn* phengite; *Pg* paragonite; *Gln* glaucophane; *Omp* omphacite; *Jd* jadeite; *Rt* rutile; *Zrn* zircon; *Ab* albite; *Mt* magnetite; *Cld* chloritoid; *Ep* epidote; *Sph* sphene; *Ank* ankerite; *Chl* chlorite

14–44 in samples north of the VSZ. The values in column 5 of Table 2 are the standard deviations of the analyses on a single grain which, when compared to the expected standard deviations based on Poisson statistics (column 6), provide a measure of grain homogeneity (homogeneous grains are indicated in bold). As can be seen, most of the grains are statistically homogeneous in Zr concentration. Furthermore, given the observed range in Zr concentrations in the entire suite of samples (13–44 ppm) and the 2 sigma Poisson uncertainty of ± 14–26 ppm, depending on the sample, it can be concluded that the Zr concentrations are statistically homogeneous within a sample and that there is not a significant difference in Zr concentrations between samples. Most importantly, there is no statistically significant difference in the Zr concentrations in rutile between samples south and north of the VSZ.

Values of Ti in quartz (Table 3) range from 200 to 440 ppb for samples south of the VSZ and 100–550 ppb for samples north of the. Images showing the location of analysis spots are provided in the supplemental materials. In all cases, the grains with the highest concentrations of Ti also have the largest standard deviations, which suggests that the grains with the higher measured concentrations may be somewhat heterogeneous or, more likely, the analysis incorporated an inclusion of another material, thus skewing the result. It should be noted that the standard deviations reported in column 9 are based on Poisson counting statistics. These values range from 10 to 120 ppb, but it should not be inferred that these values reflect the accuracy of the analyses, which are also a function of sample characteristics (e.g., inclusion density, etc.) and standardization. For the purposes of the present paper, it is estimated that the accuracy of the analyses is approximately 100 ppb. Consequently, it may be concluded that all quartz crystals analyzed have nearly identical Ti contents and there does not appear to be any statistically significant difference in the Ti concentrations of quartz from samples south or north of the VSZ.

Figure 2 shows P–T diagrams on which isopleths of Ti-in-quartz (TitaniQ: Osborne et al. 2022) and Zr-in-rutile (ZiR: Tomkins et al. 2007) have been plotted. Calculation of P–T isopleths for both thermometers requires assumptions about the activities of TiO_2 for the TitaniQ thermometer and ZrO_2 for the ZiR thermometer. All samples studied contain quartz and zircon, so the activity of ZrO_2 as defined by the equilibrium $ZrSiO_4 = ZrO_2 + SiO_2$ is unity. The activity of TiO_2 requires evaluation of the stability of rutile and, as will be

Table 2 Zr-in-rutile analyses for blueschist samples from Sifnos, Greece

1	2	3	4	5	6	7
	Grain	No. Spots[1]	Zr ppm	1 σ (s.d.) [3]	Exp s.d [2]	Notes
Samples south of the Vroulidia shear zone						
SPH99-1c	1	11	**19**	**8**	**9**	Matrix
	2	8	29	12	9	Matrix
	3	7	**34**	**6**	**9**	Matrix
	4	5	40	11	9	Matrix: garnet rim
	5	3	**18**	**9**	**9**	Inclusion: garnet
	6	5	**23**	**8**	**9**	Inclusion: garnet
	7	10	19	10	9	Inclusion: garnet
SPH99-2	1	4	39	13	9	Matrix
	3	5	**35**	**10**	**9**	Matrix: garnet rim
	4	5	**22**	**3**	**9**	Inclusion: garnet
	5	5	**22**	**8**	**9**	Inclusion: garnet
	6	3	26	12	9	Inclusion: garnet
	7	5	**27**	**4**	**9**	Inclusion: garnet
SPH99-3	1	10	38	11	9	Matrix: garnet rim
	2	10	**33**	**9**	**9**	Matrix: garnet rim
	3	10	38	14	9	Inclusion: garnet
	4	2	**24**	**3**	**7**	Matrix: garnet rim
	5	5	20	9	7	Matrix
	6	3	**27**	**6**	**7**	Matrix: garnet rim
	7	4	**15**	**5**	**7**	Inclusion: garnet
	8	3	**13**	**2**	**7**	Inclusion: garnet
SPH99-5	1	3	**31**	**11**	**13**	Inclusion: garnet rim
	2	3	**22**	**10**	**13**	Inclusion: garnet rim
	3	3	**31**	**11**	**13**	Inclusion: garnet core
	4	4	23	15	13	Matrix
	5	3	**43**	**9**	**13**	Matrix
	6	4	41	18	13	Inclusion: garnet
	7	3	**38**	**11**	**13**	Inclusion: garnet
	8	1	29		13	Matrix
SPH-150	1	4	25	18	7	Inclusion: garnet margin
	2	1	29		7	Inclusion: garnet core
	3	4	**23**	**4**	**7**	Inclusion: garnet core
	4	3	**23**	**7**	**7**	Inclusion: garnet core
	5	4	32	12	7	Inclusion: garnet core
	6	4	**27**	**3**	**7**	Matrix: garnet rim
	7	2	**22**	**1**	**7**	Matrix
	8	5	34	8	7	Matrix
Samples north of the Vroulidia shear zone						
SPH-148a	1	2	26	17	13	Inclusion: garnet
	4	2	**22**	**9**	**13**	Inclusion: garnet
	5	3	**22**	**3**	**13**	Inclusion: garnet
	6	3	**24**	**5**	**13**	Inclusion: garnet
SPH-148c	1	3	17	12	9	Inclusion: garnet
	2	3	14	13	9	Inclusion: garnet
	3	2	**40**	**5**	**9**	Inclusion: garnet
	4	5	24	16	9	Inclusion: garnet
	5	2	15	11	9	Inclusion: garnet
SPH-149c	1	4	**22**	**8**	**13**	Inclusion: garnet
	2	5	**15**	**6**	**13**	Inclusion: garnet
	3	4	**15**	**11**	**13**	Inclusion: garnet

Table 2 (continued)

Samples north of the Vroulidia shear zone						
	4	7	**21**	**7**	**13**	Inclusion: garnet
	5	5	**24**	**10**	**13**	Matrix: garnet rim
	6	3	**23**	**5**	**13**	Matrix
	7	4	**19**	**8**	**13**	Inclusion: garnet
SPH-149d	1	27	**33**	**7**	**7**	Matrix
	2	11	**36**	**6**	**7**	Inclusion: garnet
	3	7	**34**	**5**	**7**	Inclusion: garnet
	4	12	33	8	7	Martix: garnet rim
	5	7	**34**	**4**	**7**	Matrix: pseudomorph
	6	8	31	8	7	Matrix: pseudomorph
	7	86	30	9	7	Matrix
	8	62	**34**	**7**	**7**	Matrix
[4]	9	1	35.8		1	Matrix
[4]	10	1	36.4		1	Matrix
SPH99-7	1	7	**14**	**7**	**13**	Inclusion: garnet
	2	2	**23**	**4**	**13**	Inclusion: garnet
	5	7	**20**	**8**	**7**	Inclusion: garnet
	6	8	28	11	7	Inclusion: garnet
	7	7	**26**	**6**	**7**	Inclusion: garnet
	8	8	**18**	**6**	**7**	Inclusion: garnet
SPH99-8a	1	2	**24**	**7**	**13**	Inclusion: garnet
	3	3	44	26	13	Inclusion: garnet
	4	4	**38**	**13**	**13**	Matrix: garnet rim
	5	6	**37**	**13**	**13**	Matrix
SPH99-8b	6	6	32	18	13	Matrix: garnet rim
	7	2	**14**	**10**	**13**	Inclusion: garnet
	10	6	32	18	13	Matrix
	11	4	**30**	**9**	**13**	Matrix
	12	5	**18**	**5**	**13**	Matrix

[1]Number of analyses = No Spots*4 (four simultaneous spectrometer analyses)

[2]Expected standard deviation calculated from Poisson statistics for three analysis protocols: ± 13 ppm = 100 na and 120 s; ± 9 ppm = 200 na and 120 s; ± 7 ppm = 200 na and 200 s

[3]s.d. is standard deviation (measured) of all analyses for a grain. Compare with expected s.d. to ascertain homogeneity of grain. Statistically homogeneous grains are indicated in bold text

[4]Analyses by SIMS. All other analyses by electron microprobe

discussed below, quartz is not interpreted to have recrystallized with rutile present. All isopleths of TitaniQ shown in Fig. 2 were calculated assuming the activity of TiO_2 was unity, and a more rigorous analysis will be presented below.

As can be seen, the data from south and north of the VSZ are quite similar and both show an intersection at around 475–500 °C, 2.2–2.4 GPa. The lines with gentle slopes are isomekes from quartz-in-garnet barometry (QuiG) based on values reported in Castro and Spear (2017) for three samples and the experimental calibration of Thomas and Spear (2018). The difference in pressure of garnet formation between samples south and north of the VSZ is clearly evident in the QuiG results, as discussed by Castro and Spear (2017). Of particular significance is the observation that the intersection of TitaniQ and ZiR in the northern sample is entirely consistent with the P–T conditions inferred for garnet formation from QuiG (black squares) whereas for the two southern samples, the intersection falls at significantly higher pressure.

The irregular lines are the equilibrium phase boundaries for rutile stability calculated from the bulk compositions given in Table 4. The solid boundaries are calculated using

Table 3 Ti-in-quartz analyses

Sample	Position[2]	40/30	stdev	48/30	stdev	48/30(corr)	Ti(ppb)	Stdev[1]
South of the Vroulidia shear zone								
SPH99-1C/A	Inclusion	6.29E–03	2.00E–03	5.49E–05	1.50E–05	4.33E–05	440	120
	Inclusion	4.75E–03	7.90E–04	3.19E–05	3.90E–06	2.31E–05	240	30
SPH99-1C/B	Matrix	3.99E–03	6.70E–04	2.86E–05	6.80E–06	2.12E–05	220	50
	Matrix	4.00E–03	6.50E–04	2.73E–05	2.60E–06	1.99E–05	200	20
	Matrix	5.78E–03	3.90E–04	4.60E–05	1.20E–05	3.53E–05	360	90
SPH99-2/C	Matrix	4.32E–03	5.60E–04	4.80E–05	6.30E–06	4.00E–05	410	50
	Matrix	3.72E–03	5.40E–04	4.41E–05	4.30E–06	3.72E–05	380	40
	Matrix	2.87E–03	4.40E–04	2.82E–05	3.80E–06	2.29E–05	230	30
SPH99-3/A	Inclusion	5.81E–03	**	4.00E–05	7.40E–06	2.93E–05	300	60
	Inclusion	5.52E–03	**	3.79E–05	7.80E–06	2.77E–05	280	60
	Inclusion	1.06E–02	**	5.67E–05	1.70E–05	3.71E–05	380	110
SPH-150/A	Matrix	4.24E–03	9.00E–04	4.66E–05	1.40E–05	3.87E–05	400	120
	Matrix	3.51E–03	6.50E–04	3.04E–05	1.02E–05	2.39E–05	250	80
	Matrix	3.69E–03	6.60E–04	3.40E–05	4.70E–06	2.72E–05	280	40
	Matrix	3.53E–03	6.90E–04	3.18E–05	5.70E–06	2.52E–05	260	50
North of the Vroulidia shear zone								
SPH-149C/A	Matrix	4.64E–03	9.00E–04	6.18E–05	9.70E–06	5.32E–05	550	90
	Matrix	4.21E–03	8.60E–04	5.38E–05	3.60E–06	4.60E–05	470	30
	Matrix	3.28E–03	6.90E–04	2.53E–05	4.00E–06	1.92E–05	200	30
SPH-149C/B	Inclusion	4.99E–03	**	3.91E–05	8.50E–06	2.99E–05	310	70
	Inclusion	5.36E–03	8.40E–04	6.09E–05	1.26E–05	5.10E–05	520	110
SPH-149C/C	Matrix	4.01E–03	7.00E–04	5.77E–05	9.30E–06	5.02E–05	520	80
	Matrix	3.61E–03	6.40E–04	3.92E–05	6.70E–06	3.25E–05	330	60
SPH-149C/D	Inclusion	4.63E–03	7.70E–04	6.00E–05	1.40E–05	5.14E–05	530	120
	Inclusion	2.89E–03	5.10E–04	4.12E–05	7.20E–06	3.59E–05	370	60
SPH99-8B/A	Matrix	2.86E–03	7.00E–04	2.62E–05	5.40E–06	2.09E–05	210	40
	Matrix	2.92E–03	6.70E–04	2.34E–05	4.90E–06	1.80E–05	180	40
	Matrix	2.56E–03	4.40E–04	2.24E–05	5.60E–06	1.76E–05	180	40
	Matrix	2.68E–03	5.60E–04	2.22E–05	4.30E–06	1.72E–05	180	30
SPH99-8B/B	Matrix	2.28E–03	4.00E–04	1.89E–05	3.50E–06	1.47E–05	150	30
	Matrix	2.08E–03	4.40E–04	2.14E–05	3.30E–06	1.75E–05	180	30
	Matrix	1.71E–03	3.40E–04	1.87E–05	1.68E–06	1.55E–05	160	10
SPH99-8B/C	Matrix	9.01E–04	1.30E–04	1.19E–05	2.14E–06	1.02E–05	100	20
	Matrix	2.53E–03	3.70E–04	1.78E–05	3.40E–06	1.31E–05	130	30
	Matrix	2.90E–03	6.30E–04	2.68E–05	5.70E–06	2.15E–05	220	50
	Matrix	2.13E–03	3.40E–04	1.88E–05	2.90E–06	1.49E–05	150	20
	Matrix	1.98E–03	3.80E–04	2.67E–05	4.30E–06	2.30E–05	240	40

Ca correction: $^{48}Ca/^{40}Ca = 0.00185$

Working curve 1: Ti(ppm) = 1.028e4*(48/30)corrected

Working curve 2: Ti(ppm) = 1.13e4*(48/30)corrected

**No s.d. available

[1]Stdev based on Poisson counting statistics

[2]Quartz grains are either in the matrix or inclusions within garnet

the thermodynamic dataset of Spear and Pyle (2010) (SPaC), the dashed and dotted lines were calculated using the values from Holland and Powell (1998: HP98) and (2011: HP11), respectively, with datasets ds5.5 and ds6.2, respectively. The calculations using the HP98 and HP11 datasets place rutile stability at somewhat higher pressure and/or temperature

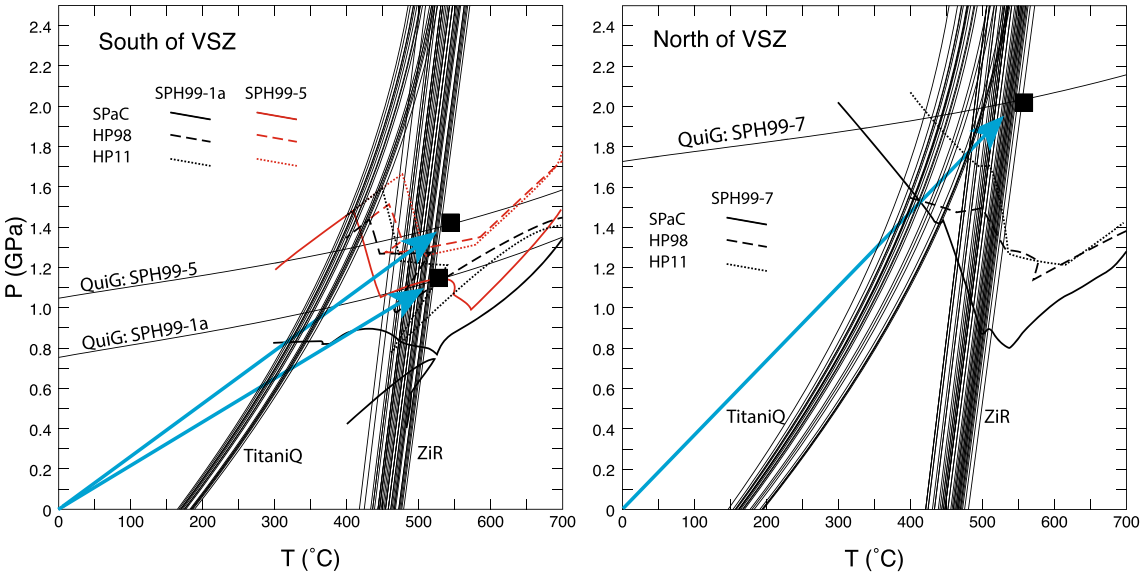

Fig. 2 Pressure–temperature diagrams showing the results of Ti-in-quartz (TitaniQ), Zr-in-rutile (ZiR), and quartz-in-garnet (QuiG) thermobarometry for (**a**) samples south of the Vroulidia shear zone (VSZ) and (**b**) the sample north of the VSZ. Irregular lines are the locations of the rutile-in reaction for each sample calculated using the thermodynamic data sets of Spear and Pyle (2010: SPaC—solid lines), Holland and Powell (1998: HP98 with ds5.5—dashed lines) and Holland and Powell (2011: HP11—dotted lines). Blue arrows show metamorphic trajectories discussed in the text. Black squares are the inferred conditions of garnet formation after Castro and Spear (2017) and are interpreted as representing the peak metamorphic conditions

Table 4 Bulk rock analyses used in calculations

	SPH99-1a	SPH99-5	SPH99-7
SiO_2	76.00	75.18	55.44
Al_2O_3	12.72	11.42	17.32
TiO_2	0.37	0.27	0.35
MgO	1.03	0.63	5.08
FeO	3.26	5.94	7.95
MnO	0.11	0.04	0.13
CaO	0.95	1.42	5.32
Na_2O	3.83	4.83	5.31
K_2O	1.88	0.54	2.25
H_2O*	10.00	10.00	10.0

Composition determined from EDS analysis of entire thin section

*Sufficient H_2O was added to each bulk composition to ensure excess fluid at all P–T conditions

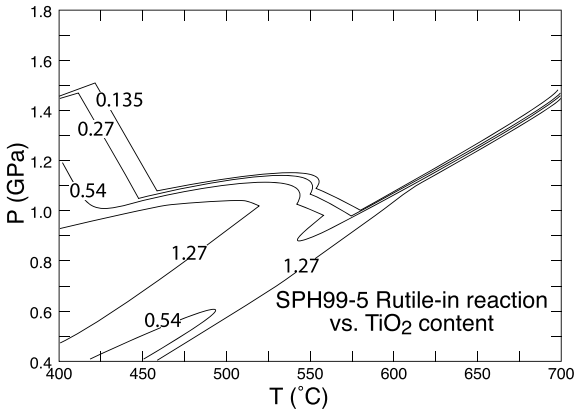

Fig. 3 Pressure–temperature diagram showing the sensitivity of the calculated rutile-in reaction to the bulk rock TiO_2 content. Values on the curves are the TiO_2 content in wt.%. Calculations were done using the SPaC thermodynamic dataset

than the SPaC dataset and the implications of this will be discussed below.

The location of the equilibrium phase boundary for rutile is, of course, also a function of the bulk rock TiO_2 content. To explore the sensitivity of the rutile-in reaction, calculations have been performed using the measured TiO_2 content (0.27 wt.%), one-half of this value (0.135 wt.%), twice this value (0.54 wt.%) and 1.0 wt.% larger (1.27 wt.%) (Fig. 3). Within a factor of 2 of the measured TiO_2 content, the equilibrium phase boundary for rutile varies only minor amounts.

Discussion

QuiG results

To compare the results of the TitaniQ and ZiR results with the inferred peak metamorphic conditions, it is necessary to evaluate as accurately as possible the peak metamorphic condition. Castro and Spear (2017) used a combination of QuiG barometry, ZiR thermometry and thermodynamic

calculations (mineral assemblage diagrams or MADs) to infer the peak P–T conditions. The peak pressure was primarily constrained by the results of inclusion barometry (QuiG) and the proper application of this method has been the subject of considerable discussion (e.g., Angel et al. 2019; Murri et al. 2018). Castro and Spear (2017) employed the so-called "hydrostatic method" by which the pressure on the quartz inclusion was determined from the Raman shift of the 464 cm^{-1} peak using the calibration of Schmidt and Ziemann (2000) and the elastic model of Guiraud and Powell (2006). Angel et al. (2019) have argued that the Raman shifts are actually the result of strain on the inclusion and have presented theoretical and practical approaches to calculate these strains. We have analyzed both methods using the experimental data in Thomas and Spear (2018) and the analysis is presented in the supplemental material (S1 Supplemental Material). We found that the hydrostatic method reproduces the experimental pressures well at low pressure (1 GPa) but there is an increasing deviation between the experimental and hydrostatic pressures with increasing pressure up to 2 GPa. In contrast, the elastic tensor method results in systematic overestimate of the experimental pressures by approximately 0.17 GPa. For the present study, we have recalculated the QuiG results using both the hydrostatic and elastic tensor methods with the addition of the peak shifts for the 206 and 128 cm^{-1} data for the samples used by Castro and Spear (2017). The results are presented in Table 5 and shown in Figs. 4, 5 and 6. As can be seen, the difference in QuiG pressures calculated by the two different methods does not alter the interpretations in this paper.

Crystallization along subduction P–T paths

To evaluate the consistency and significance of the TitaniQ and ZiR results with respect to calculated quartz and rutile stability fields, linear subduction P–T paths have been drawn in Figs. 2, 4, 5 and 6 that correspond to metamorphic P–T trajectories that intersect the peak P–T conditions (blue arrows). These are, for samples SPH99-1a, SPH99-5, and SPH99-7 approximately 22, 26 and 36 bar/deg, respectively (12.1, 10.2, and 7.4 deg/km, respectively). Other metamorphic P–T paths are, of course, possible, but these represent the simplest and form a basis for discussion and comparison. Also shown in Figs. 4, 5 and 6 are contours for the calculated rutile-in reaction (red lines with affinity = 0.0), the affinity of rutile above the rutile-in reaction (black lines with positive values), and the affinity of rutile below the rutile-in reaction (blue lines with negative values). These latter contours will be used below to assess the activity of TiO_2 where rutile is not stable.

An important consideration before evaluating the significance of the TitaniQ and ZiR results is whether the Ti contents of the quartz or Zr contents of rutile were substantially modified subsequent to formation by either diffusion or dynamic recrystallization. Using the diffusivities from Cherniak et al. (2007a), the diffusion distance ($X = \sqrt{Dt}$) for Ti in quartz at 550 °C (the upper bound of the inferred peak T) is only 3.3 µm in 1 ma and 10 µm in 10 Ma. The lack of Ti resetting by diffusion at temperatures up to the middle amphibolite facies is also consistent with CL imaging of Ti in quartz reported by Spear and Wark (2009) and Ashley et al. (2013). A similar calculation for Zr in rutile using the diffusivities of Cherniak et al. (2007b) indicate that the characteristic diffusion distance $X = \sqrt{Dt}$) at 550 °C are only 2 and 6 µm in 1 and 10 Ma, respectively, which is even shorter than the characteristic distance for quartz diffusion. It is therefore concluded that the Ti and Zr contents of quartz and rutile, respectively, have not been substantially modified by diffusion. The absence of chemical zoning in quartz and rutile also supports this conclusion.

A number of studies have documented the modification of Ti concentrations in quartz as a result of dynamic recrystallization, for example in mylonites (e.g., Kohn and Northrup 2009; Grujic et al. 2011; Nachlas, et al. 2014, 2018; Nachlas and Hirth 2015; Bestmann and Pennacchioni 2015). The

Table 5 Maximum shift of quartz inclusions in garnet for samples in this study

Sample	T	464[1]	206[1]	128[1]	e1 + e2[2]	e3[2]	Pinc Elastic Tensor[3]	Ptrap at T[5]	Ptrap at T corrected	464 Pinc Hydro[3,4]	Ptrap at T[6]
SPH99-1a	525	4.28	12.79	2.79	− 0.017426	0.0006066	0.584	1.435	1.248	0.476	1.151
SPH99-5	525	5.50	16.59	4.05	− 0.019570	− 0.0010572	0.730	1.699	1.509	0.615	1.360
SPH99-7	530	8.45	22.09	6.49	− 0.013951	− 0.0097045	0.906	2.035	1.840	0.955	1.908

[1]Uncertainties are 464 (0.3), 206 (1.0), 128 (0.3). Raman shifts are cm^{-1}

[2]Correlation coefficients are − 98.7

[3]Pressures are in GPa

[4]Hydrostatic model after Schmidt and Zieman (2000)

[5]Calculated using program EntraPT (Mazzucchelli et al. 2021)

[6]Calculated after Guiraud and Powell (2006)

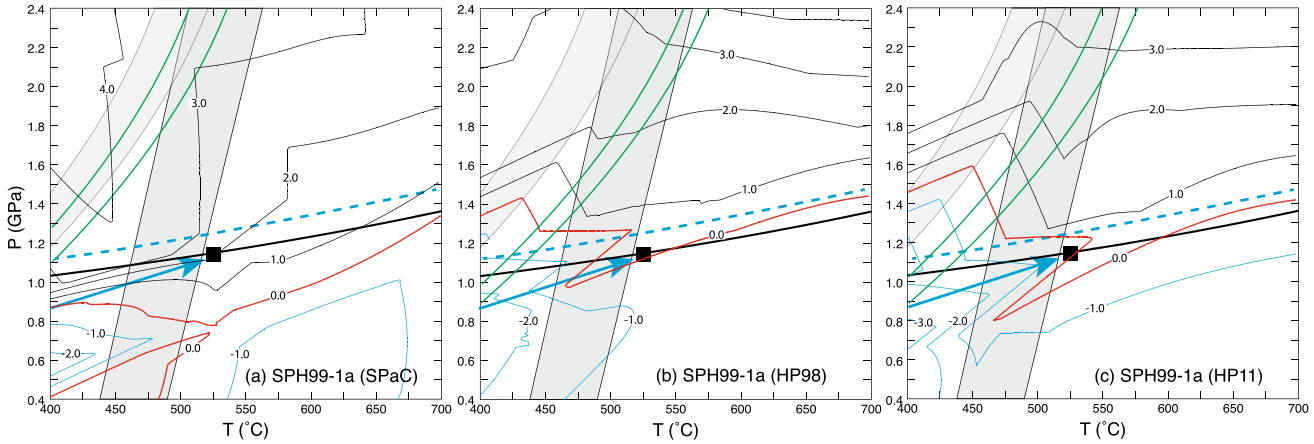

Fig. 4 Pressure–temperature diagrams showing results of calculations for sample SPH99-1a (south of the VSZ). Black square is the inferred peak metamorphic condition and bold shallow line through the black square is the result of QuiG barometry (from Castro and Spear 2017). Gray bands are the show the range of P–T conditions calculated from TitaniQ and ZiR thermometry. Irregular lines are calculated values of rutile affinity based on the thermodynamic datasets (**a**) SPaC; (**b**) HP98; (**c**) HP11. Values on the contours are affinities in units of kJ/mol-O. Red contour (affinity = 0) is the rutile-in reaction, black contours are where affinity > 0 and blue contours are where affinity < 0. Blue arrows are a metamorphic gradient of 22 bar/deg (c.a. 12.1 deg/km). Green lines are the offsets of TitaniQ thermometry from calculated TiO_2 activities along the blue P–T path

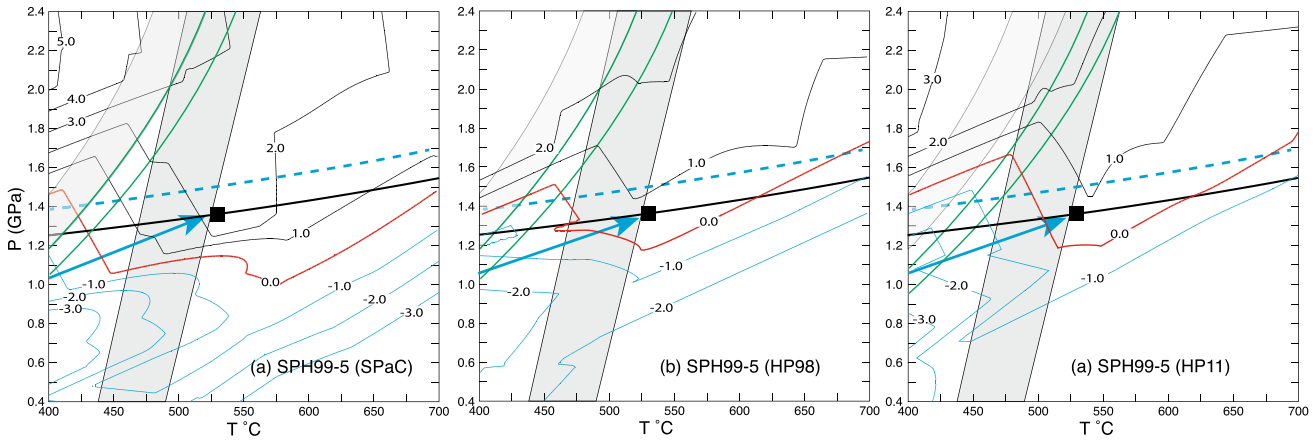

Fig. 5 Pressure–temperature diagrams showing calculations for sample SPH99-5 (south of the VSZ). Labels as in Fig. 4. Blue arrows are a metamorphic gradient of 26 bar/deg (c.a. 10.2 deg/km)

quartz grains examined in the present study do not display any evidence of late-metamorphic recrystallization or strain such as undulose extinction, deformation lamellae, mosaic textures, or grain size reduction (see images in supplemental materials). Moreover, the Ti contents of quartz inclusions within garnet are statistically identical to those of matrix grains, which would not be expected if the matrix grains had experienced dynamic recrystallization. Therefore, it is concluded that the measured concentrations reflect those at the time of formation.

TitaniQ results

For samples SPH99-1a and SPH99-5, the subduction P–T path passes through the field of the TitaniQ results at temperatures of around 300 °C (Fig. 2 and Figs. 4 and 5). These calculations were made assuming $a(TiO_2) = 1.0$ but considering that rutile is not stable at these conditions, $a(TiO_2)$ must have been less than 1.0. The activity of TiO_2 is related to the affinity contours by the relationship

$$\mu(TiO_2) = \mu^o(TiO_2) + RT \ln a(TiO_2),$$

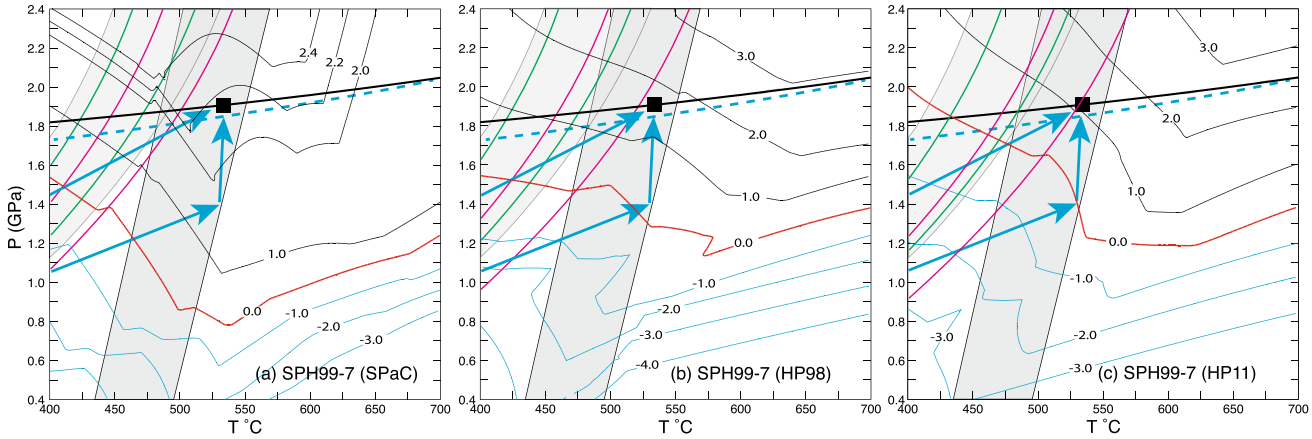

Fig. 6 Pressure–temperature diagrams showing calculations for sample SPH99-7 (north of the VSZ). Labels as in Fig. 4. Blue arrows are a metamorphic gradient of 36 bar/deg (c.a. 7.4 deg/km) and 26 bar/deg (from sample SPH99-5: Fig. 5) followed by nearly isothermal loading. Magenta lines are offset of TitaniQ temperatures with TiO_2 activities calculated along the gradient of 26 bar/deg (10 deg/km) (i.e., blue path for sample SPH99-5)

where $\mu(TiO_2)$ is the calculated chemical potential of TiO_2 based on the matrix (rutile-free) assemblage and $\mu^o(TiO_2)$ is the standard state chemical potential of rutile at the P–T conditions of consideration. Thus, $a(TiO_2)$ can be calculated from the relationship

$$a\left(TiO_2\right) = \exp(\Delta\mu/RT), \quad (1)$$

where $\Delta\mu = \mu(TiO_2) - \mu^o(TiO_2)$. At the rutile-in reaction, this value is, of course, zero.

Calculation of $a(TiO_2)$ requires the P–T conditions of quartz formation be known. Using the subduction P–T trajectories shown in blue in Figs. 4, 5 and 6, the pressure at any temperature can be calculated and the value of $\Delta\mu$ determined from the intersection of the path with the blue contours of affinity (i.e., $\Delta\mu$) and from this the activity can be calculated from Eq. 1. Note that the blue contours are in units of J/mol-O (i.e., for $Ti_{1/2}O$) whereas the value of $\Delta\mu$ used to calculate activity is in units of J/mol-TiO_2 so are twice the values shown on the contours. Activity does not vary strongly with temperature but does vary significantly with $\Delta\mu$. For example, for a value of $\Delta\mu = 1000$ J/mol over a temperature range from 300 to 500 °C the activity only varies from 0.81 to 0.85. However, changing $\Delta\mu$ from 1000 to 5000 J at 400 °C varies the activity from 0.83 to 0.41.

Based on the assumed P–T trajectory and the calculated values of $\Delta\mu$, the temperature from TitaniQ can be solved iteratively. This has been done for the highest and lowest Ti concentrations from south and north of the VSZ and the results are shown in Table 6 and Figs. 4, 5 and 6 as green lines. For example, in sample SPH99-1a (Fig. 4) the lowest and highest Ti concentration are 200 and 440 ppb, the calculated TiO_2 activities are 0.58 and 0.79 (using the SPaC thermodynamic dataset), and the corresponding temperatures from TitaniQ are 314 and 345 °C, respectively. These temperatures can be compared with calculations assuming $a(TiO_2) = 1$ of 298 and 333 °C, respectively. That is, the calculations using the revised values of $a(TiO_2)$ are 18 and 11 degrees higher. A similar calculation for sample SPH99-5 (Fig. 5) results in calculated activities of 0.46 and 0.67 and temperatures 33 and 20 degrees higher than those calculated assuming $a(TiO_2) = 1$. Similar results are obtained using the HP98 and HP11 thermodynamic datasets although the values of $a(TiO_2)$ are generally lower than that calculated from the SPaC dataset (Table 6).

Sample SPH99-7 (Fig. 6) is somewhat more problematic to interpret because the subduction P–T trajectory of 7.4 deg/km passes through the array of TitaniQ results calculated with $a(TiO_2) = 1$ and also passes into the P–T region above the rutile-in reaction (red line with affinity = 0) but apparently rutile had not yet formed based on the ZiR results. In this region (above the rutile-in reaction but below the ZiR contours) the activity of TiO_2 is greater than 1, which will have the result of lowering the calculated TitaniQ temperature from that obtained assuming $a(TiO_2) = 1$. Further complicating the calculations is the observation that the P–T trajectory enters the ZiR array near the metamorphic peak. Once rutile forms, the activity will drop from whatever elevated value it had back to 1.0. Thus, it is not clear how to correct the values with the higher Ti contents for TiO_2 activity. What has been done in Fig. 6 is to calculate the activity of TiO_2 for both the lowest and highest Ti contents (100 and 530 ppb, respectively) assuming that rutile has not formed. The result is to raise the temperature of the low-Ti measurement and lower the temperature of the high Ti measurement, thus reducing the spread (green lines in Fig. 6).

Figures 4 and 5 clearly demonstrate that the Ti concentrations in quartz from samples collected south of the VSZ

Table 6 Calculated values of activity of TiO_2, T and P for minimum and maximum Ti concentrations in quartz along assumed P–T gradients

	Min Ti (ppb)	a(TiO_2)	T °C	P (GPa)	Max Ti (ppb)	a(TiO2)	T °C	P (GPa)
SPH99-1a	Gradient = 21.9 bar/deg							
SPaC	200	0.58	314	0.688	440	0.79	345	0.757
HP98	200	0.25	373	0.817	440	0.39	397	0.871
HP11	200	0.29	362	0.793	440	0.39	399	0.874
SPH99-5	Gradient = 26.4 bar/deg							
SPaC	200	0.46	371	0.980	440	0.67	403	1.063
HP98	200	0.46	371	0.980	440	0.62	409	1.081
HP11	200	0.34	393	1.039	440	0.49	427	1.130
SPH99-7	Gradient = 36.7 bar/deg							
SPaC	100	0.72	377	1.386	530	1.41	467	1.716
HP98	100	0.78	372	1.365	530	1.31	475	1.744
HP11	100	0.612	390	1.432	0.53	1.13	492	1.806
SPH99-7	Gradient = 26.4 bar/deg (path for SPH99-5)							
SPaC	100	0.449	326	0.860	530	0.840	396	1.045
HP98	100	0.363	340	0.899	530	0.604	422	1.114
HP11	100	0.278	359	0.949	530	0.512	436	1.151

were incorporated below the peak metamorphic temperature, and likely they were locked in at a temperature around 300 °C. The interpretation of results from the sample north of the VSZ are not so clear, but if the 7.4 deg/km path is correct, it appears that the Ti concentrations in quartz were obtained prior to the metamorphic peak as well.

ZiR results

Kinetic theory requires a finite amount of overstepping to drive the nucleation of a new phase but the amount of affinity required to nucleate rutile is not known. Estimates of garnet affinity at the point of nucleation range from a couple of hundred J/mol-O to over 2000 J/mol-O (e.g., Pattison et al. 2011; Spear et al. 2014; Castro and Spear 2017; Wolfe and Spear 2018; Spear and Wolfe 2022) and it is reasonable to assume that similar values apply to rutile. Figures 4, 5, and 6 present P–T diagrams contoured for the rutile affinity in the region where rutile is nominally stable but has not yet nucleated (black contours). Regardless of the thermodynamic database used (SPaC, HP98 or HP11), the buildup of affinity above the equilibrium reaction is quite rapid. If it is assumed that the nucleation of rutile requires no more than around 1.0 kJ/mol-O, then it is possible to infer the P–T conditions of rutile formation based on the 1.0 kJ affinity contour and the ZiR results. Furthermore, to encompass all of the measured ZiR values, it is desirable that the 1.0 kJ/mol-O contour be intersected at the highest temperature recorded by the ZiR results, within uncertainty.

Comparison of the results of ZiR thermometry with the calculated values of affinity vary somewhat depending on the thermodynamic database used to calculate affinities. For sample SPH99-1a (Fig. 4) using the SPaC dataset (Fig. 4a), the suggested P–T path crosses the lowest ZiR temperature where the affinity is 1.0 kJ/mol-O and reaches the highest ZiR temperature where the affinity is 2.0 kJ/mol-O. Using the HP98 dataset (Fig. 4b), the path is nearly coincident with the rutile-in reaction (affinity = 0) and using the HP11 dataset (Fig. 4c) the temperatures recorded by ZiR are entirely below the rutile-in reaction (affinity < 0). For sample SPH99-5 (Fig. 5), a similar result is seen using the SPaC dataset (Fig. 5a) and the HP98 dataset (Fig. 5b) yields a result consistent with rutile formation with little or no overstepping. With the HP11 dataset (Fig. 5c), the ZiR temperatures fall above and below the rutile-in reaction (negative and positive affinities).

For sample SPH99-7 following the P–T trajectory of 7.4 deg/km (Fig. 6) using the SPaC dataset, ZiR temperatures are not encountered until the affinity = 1.5 kJ/mol-O whereas using the HP98 and HP11 datasets the lowest ZiR temperatures are encountered at affinities of around 1.0 kJ/mol-O and 0.0 kJ/mol-O. Thus, it would appear that calculations using the SPaC dataset are most consistent with the ZiR results and rutile formation for samples SPH99-1a and SPH99-5 but the HP98 and HP11 datasets are more consistent with results from sample SHP99-7.

An alternative scenario is proposed, however, whereby sample SPH99-7 followed an initial P–T trajectory similar to that followed by the samples south of the VSZ and subsequently encountered a phase of nearly isothermal loading. A second path consistent with this scenario is shown in Fig. 6 where the initial burial is along a trajectory at 10 deg/km (identical to sample SPH99-5) up to a temperature of around 525 ˚C followed by loading to around 2.0 GPa. Following this path, calculations using the SPaC dataset suggest rutile began to form at the rutile-in reaction (affinity = 0)

and continued to where affinity was around 1.5 kJ/mol-O. Calculations done with both the HP98 and HP11 datasets show ZiR temperatures occurring below the rutile-in reaction (affinity < 0). Offsets of the TitaniQ thermobarometer resulting from the reduced activity of TiO_2 along this path (10 deg/km) are given in Table 6 and shown in Fig. 6 as magenta lines. The TiO_2 activities are smaller along this path resulting in an increase in the calculated TitaniQ temperatures (Fig. 6), but the conclusion remains valid that the Ti contents of quartz must have been incorporated at a temperature below the metamorphic peak. Which P–T history for sample SPH99-7 is correct is difficult to say but the consistency of ZiR thermometry with calculations of rutile stability using the SPaC dataset for samples south of the VSZ suggests that these results more closely fit the observed data. Furthermore, from a tectonic perspective, it is unclear how different samples from the same subduction zone could experience initial subduction gradients that would be so radically different and it seems reasonable that all samples followed a similar initial gradient after which the region north of the VSZ underwent additional rapid burial.

Implications for the prograde P–T path and the tectonic implications

The discussion of possible sequences of phase crystallization and implications for TitaniQ and ZiR thermobarometry are valid regardless of the thermodynamic data set used (SPaC, HP98 or HP11). Most importantly, it is clear that temperatures recorded by TitaniQ do not reflect the peak temperature experienced by a sample and the preferred interpretation is that TitaniQ values reflect the temperature of early quartz recrystallization along a subduction geotherm. ZiR values are typically closer to the peak metamorphic temperature, but again, represent minimum estimates because in these samples the peak T is constrained to be higher than the ZiR temperatures at the pressures recorded by the QuiG barometer (see Castro and Spear 2017, for a detailed discussion).

Given these results, it is believed that the simplest P–T path for the prograde metamorphism of the EBU is an initial metamorphic path along a gradient similar to that recorded by samples south of the VSZ (SPH99-1 and SPH99-5) (e.g., 22–26 bar/deg or 12–10 deg/km). This type of relatively shallow geothermal gradient is to be expected during nascent subduction before significant under thrusting and down bowing of the thermal structure has occurred. It should not be inferred that the north and south units were necessarily near each other during the initial subduction, only that they followed a similar metamorphic gradient. A decoupling of units south and north of the VSZ then resulted in the rapid, nearly isothermal burial of samples north of the VSZ after which the two units were juxtaposed during exhumation.

These results should not be misconstrued to imply that all TitaniQ results from blueschists and eclogites reflect recrystallization at low temperature. A sample of eclogite from Syros, Greece, has Ti concentrations in quartz that range from 4.7 to 62.5 ppm, which correspond to temperatures at 2.0 GPa of 660 to 910 °C. Inasmuch as the peak P–T conditions for this eclogite are around 550 °C, 2.0 GPa, these Ti values cannot reflect quartz recrystallization at either the peak metamorphic conditions or those obtained along a prograde subduction path. Rather, it is likely that that they are relict from the original igneous protolith.

In conclusion, then, the above discussion illustrates that the TitaniQ and ZiR thermobarometers do not necessarily record peak metamorphic conditions but rather record conditions along the prograde metamorphic gradient. A similar conclusion regarding the significance of TitaniQ thermometry was reached for regionally metamorphosed schists of central Vermont by Ashley et al. (2013). Of course, at higher temperatures where diffusional modification of initial Ti and Zr contents occurs, this generalization is no longer valid and Ti and Zr values in quartz and rutile can take on complex zoning as a function of thermal history, TiO_2 and ZrO_2 activities, and grain boundary mobilities (e.g., Spear and Wark 2009; Kohn et al. 2016).

Supplementary Information The online version contains supplementary material available at https://doi.org/10.1007/s00410-022-01989-4.

Acknowledgements This work has been supported by grants from the National Science Foundation 1447468 and 1750674 (to Spear) and the Edward P. Hamilton Distinguished Professor Chair (Rensselaer). Insightful reviews by Z. Osborne and two anonymous reviewers greatly improved the presentation of the manuscript.

Data availability statement All data generated or analysed during this study are included in this published article (and its supplementary information files).

References

Angel RJ, Murri M, Mihailova B, Alvaro M (2019) Stress, strain, and Raman shifts. Zeitschrift für Kristallographie-Crystalline Materials 234:129–140

Ashley KT, Webb LE, Spear FS, Thomas JB (2013) P-T-D histories from quartz: a case study of the application of the TitaniQ thermobarometer to progressive fabric development in metapelites. Geochem Geophys Geosyst 14(9):3821–3843. https://doi.org/10.1002/ggge.20237

Bestmann M, Pennacchioni G (2015) Ti distribution in quartz across a heterogeneous shear zone within a granodiorite: the effect of deformation mechanism on Ti resetting. Lithos 227:37–56

Castro AE, Spear FS (2017) Reaction overstepping and reevaluation of the peak P-T conditions of the blueschist unit Sifnos, Greece: implications for the Cyclades subduction zone. Int Geol Rev 59:548–562

Cherniak DJ, Manchester J, Watson EB (2007a) Zr and Hf diffusion in rutile. Earth Planet Sci Lett 261:267–279

Cherniak DJ, Watson EB, Wark DA (2007b) Ti diffusion in quartz. Chem Geol 236:65–74
Grujic D, Stipp M, Wooden JL (2011) Thermometry of quartz mylonites: importance of dynamic recrystallization on Ti-in-quartz reequilibration. Geochem Geophys Geosyst 12:19
Guiraud M, Powell R (2006) P–V–T relationships and mineral equilibria in inclusions in minerals: Earth and Planetary Science Letters 244(3-4):683–694
Holland TJB, Powell R (1998) An internally-consistent thermodynamic dataset for phases of petrological interest. J Metamorph Geol 16:309–343
Holland TJB, Powell R (2011) An improved and extended internally consistent thermodynamic dataset for phases of petrological interest, involving a new equation of state for solids. J Metamorph Geol 29:333–383
Kohn MJ, Northrup CJ (2009) Taking mylonites' temperatures. Geology 37(1):47–50. https://doi.org/10.1130/g25081a.1
Kohn MJ, Penniston-Dorland SC, Ferreira JCS (2016) Implications of near-rim compositional zoning in rutile for geothermometry, geospeedometry, and trace element equilibration. Contributions Mineral Petrol 171:15
Mazzucchelli ML, Angel RJ, Alvaro M (2021) EntraPT: an online platform for elastic geothermobarometry. Am Miner 106:830–837
Murri M, Mazzucchelli ML, Campomenosi N, Korsakov AV, Prencipe M, Mihailova BD, Scambelluri M, Angel RJ, Alvaro M (2018) Raman elastic geobarometry for anisotropic mineral inclusions. Am Miner 103:1869–1872
Nachlas WO, Hirth G (2015) Experimental constraints on the role of dynamic recrystallization on resetting the Ti-in-quartz thermobarometer. J Geophys Res 120:8120–8137
Nachlas WO, Whitney DL, Teyssier C, Bagley B, Mulch A (2014) Titanium concentration in quartz as a record of multiple deformation mechanisms in an extensional shear zone. Geochem Geophys Geosyst (G3) 15:1374–1397
Nachlas WO, Thomas JB, Hirth G (2018) TitaniQ deformed: experimental deformation of out-of-equilibrium quartz porphyroclasts. J Struct Geol 116:207–222
Osborne ZR, Thomas JB, Nachlas WO, Angel RJ, Hoff CM, Watson EB (2022) TitaniQ revisited: expanded and improved Ti-in-quartz solubility model for thermobarometry. Contributions Mineral Petrol 177:21
Pattison DRM, de Capitani C, Gaidies F (2011) Petrological consequences of variations in metamorphic reaction affinity. J Metamorph Geol 29(9):953–977. https://doi.org/10.1111/j.1525-1314.2011.00950.x
Roche V, Laurent V, Cardello GL, Jolivet L, Scaillet S (2016) Anatomy of the Cycladic Blueschist Unit on Sifnos Island (Cyclades, Greece). J Geodyn 97:62–87
Schmidt C, Ziemann MA (2000) In-situ Raman spectroscopy of quartz: a pressure sensor for hydrothermal diamond-anvil cell experiments at elevated temperatures. Am Miner 85(11–12):1725–1734
Spear FS, Pyle JM (2010) Theoretical modeling of monazite growth in a low-Ca metapelite. Chem Geol 273(1–2):111–119. https://doi.org/10.1016/j.chemgeo.2010.02.016
Spear FS, Wark DA (2009) Cathodoluminescence imaging and titanium thermometry in metamorphic quartz. J Metamorph Geol 27:187–205
Spear FS, Wolfe OM (2022) Nucleation theory applied to the development of contrasting garnet crystal densities. Contributions to Mineral Petrol 177:17
Spear FS, Wark DA, Cheney JT, Schumacher JC, Watson EB (2006) Zr-in-Rutile Thermometry in Blueschists from Sifnos, Greece. Contributions Mineral Petrol 152:375–385
Spear FS, Thomas JB, Hallett BW (2014) Overstepping the garnet isograd: a comparison of QuiG barometry and thermodynamic modeling. Contrib Miner Petrol 168(3):1–15. https://doi.org/10.1007/s00410-014-1059-6
Thomas JB, Spear FS (2018) Experimental study of quartz inclusions in garnet at pressures up to 3.0 GPa: evaluating validity of the quartz-in-garnet inclusion elastic thermobarometer. Contributions Mineral Petrol 173:14
Thomas JB, Watson EB, Spear FS, Shemella PT, Nayak SK, Lanzirotti A (2010) TitaniQ under pressure: the effect of pressure and temperature on Ti-in-quartz solubility. Contrib Miner Petrol 160:743–759
Tomkins HS, Powell R, Ellis DJ (2007) The pressure dependence of the zirconium-in-rutile thermometer. J Metamorph Geol 25:703–713
Wolfe OM, Spear FS (2018) Determining the amount of overstepping required to nucleate garnet during barrovian regional metamorphism, Connecticut Valley Synclinorium. J Metamorph Geol 36:79–94